Journal of Medical Systems (2019) 43:332
https://doi.org/10.1007/s10916-019-1455-6

IMAGE & SIGNAL PROCESSING

Lung Nodule Detection based on Ensemble of Hand Crafted and Deep Features

Tanzila Saba[1] · Ahmed Sameh[1] · Fatima Khan[1] · Shafqat Ali Shad[2] · Muhammad Sharif[3]

Received: 19 February 2019 / Accepted: 10 September 2019

Abstract

Lung cancer is considered as a deadliest disease worldwide due to which 1.76 million deaths occurred in the year 2018. Keeping in view its dreadful effect on humans, cancer detection at a premature stage is a more significant requirement to reduce the probability of mortality rate. This manuscript depicts an approach of finding lung nodule at an initial stage that comprises of three major phases: (1) lung nodule segmentation using Otsu threshold followed by morphological operation; (2) extraction of geometrical, texture and deep learning features for selecting optimal features; (3) The optimal features are fused serially for classification of lung nodule into two categories that is malignant and benign. The lung image database consortium image database resource initiative (LIDC-IDRI) is used for experimentation. The experimental outcomes show better performance of presented approach as compared with the existing methods.

Keywords Cells · Texture · Benign · VGG 19 · SVM

Introduction

During the normal growth in humans, new cells are created by following a regular pattern of dividing and dying. The uncontrolled cells growth, however, leads to cancer [1, 2]. In lung cancer, the growth rate of abnormal cells increases rapidly and creates a lump in the inner portion of lung called lung nodule. Lung nodules are in the form of spherical abnormal tissues with a 30 mm diameter approximately [3]. Lung nodule detection is essential for the patient's treatment [4]. Due to smaller size and complex pattern, it becomes a challenge to spot lung nodule at an initial phase. Lung cancer is more fatal as compared to other types of cancers [5]. Various medical scans are used to diagnose the lung cancer such as magnetic resonance imaging (MRI) [6–9], computed tomography (CT) [10] and positron emission tomography (PET) [11]. Among all these, CT scan is cost effective to diagnose lung nodule more precisely. The fast multi-detector row CT scanner scans the whole chest within a few seconds. This also generates high quality scans with isotropic voxels. CT scan shows a clear difference between normal and abnormal tissues and makes it possible to visualize the low or small opacity nodules that are hardly seen in other traditional medical imaging modalities [2, 12]. In the process of CT scan, more than one hundred slices are generated for a single case of a patient. Manually analyzing all slices and identifying the affected region is more time consuming and error prone task for the radiologists. The machine learning methods are there for lung nodules detection that provides help to radiologists for more accurate

This article is part of the Topical Collection on *Image & Signal Processing*

✉ Tanzila Saba
tsaba@psu.edu.sa

✉ Muhammad Sharif
sharif@ciitwah.edu.pk

Ahmed Sameh
asameh@psu.edu.sa

Fatima Khan
fkhan@psu.edu

Shafqat Ali Shad
shadsh01@luther.edu

[1] College of Computer and Information Sciences, Prince Sultan University, Riyadh 11586, Saudi Arabia

[2] Department of Computer Science, Luther College, Decorah, IA, USA

[3] Department of Computer Science, COMSATS University Islamabad, Wah Campus, Islamabad, Pakistan

Published online: 08 November 2019

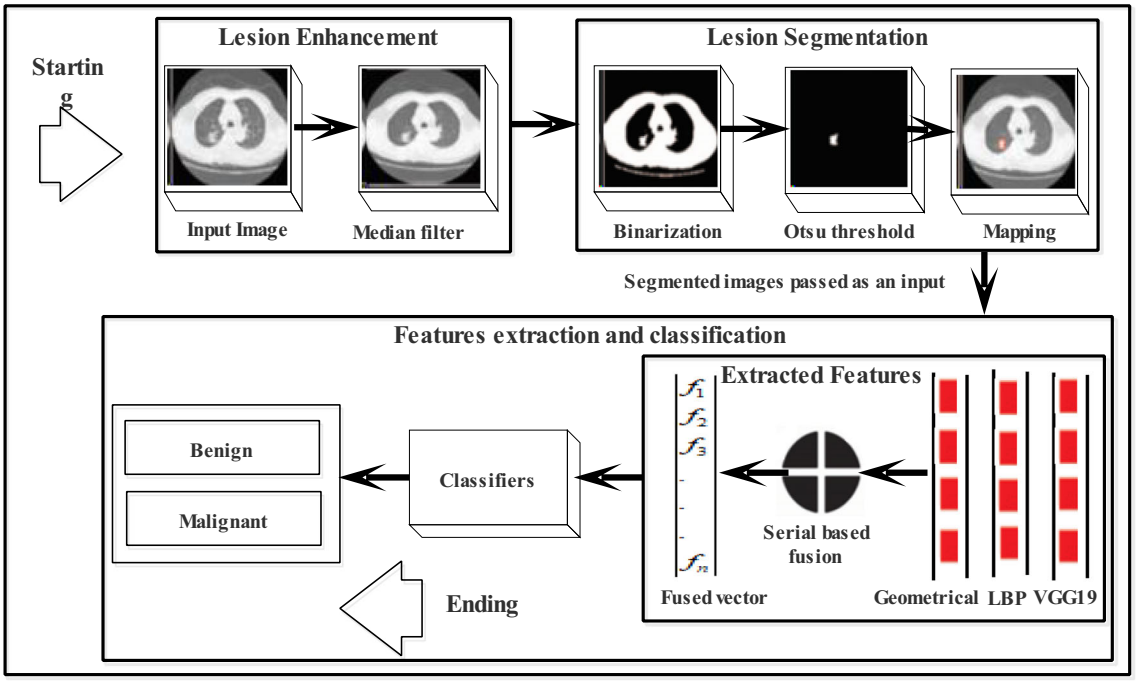

Fig. 1 Block diagram of proposed approach which shows lesion enhancement, segmentation, feature extraction and classification (where median filter is used for image smoothing, binarization is applied for lung volume extraction, Otsu threshold is utilized to segment actual lung nodule, segmented region is mapped, geometrical and texture (LBP) and deep learning features (VGG 19) are extracted and fused serially, PCA is applied to select optimal features and final fused vector is fed to classifiers to classify the benign and malignant images)

diagnosis [13, 14]. The major contribution of this manuscript is defined below:

I. Otsu algorithm is applied using the morphological operation for lung nodule segmentation.
II. The handcrafted (geometrical, texture) and deep features are extracted using a visual geometry group (VGG-19). Then, the optimal feature set is obtained using the PCA, which is further serially fused for classification

Related work

Several existing computer-aided diagnosis (CAD) methods are used to segment and predict lung [15]. The precise segmentation is an important and complicated task [16]. A number of segmentation methods are used to segment the lung nodules such as template matching [17, 18], watershed [19], vector levels of quantization [20], k-means clustering [21], lung wall template matching (LWTM) [22], Graph cuts with Gaussian mixture models [23], region growing [24], 3D template matching [25], thresholding [26, 27] and adaptive fuzzy thresholding with active contour [28].

The core of the classification process is the provision of discriminative features, which enhances the model learning to unseen data. Few of the state-of-art feature descriptors are 3D local geometry, statistical intensity [29], geometric, texture [30], shape [31, 32] and intensity [33, 34]. All these handcrafted features are commonly utilized for the prediction of lung nodule. Similarly, deep features have been extracted from each CT image using deep residual, curriculum and transfer learning architectures [35], multi-level 3Dconvolutional neural network (CNN) [36], CNN [12, 15], deep Boltzmann machine (DBM),

(a) (b) (c)

Fig. 2 Lesion Enhancement **a** input image **b** grayscale **c** median filter

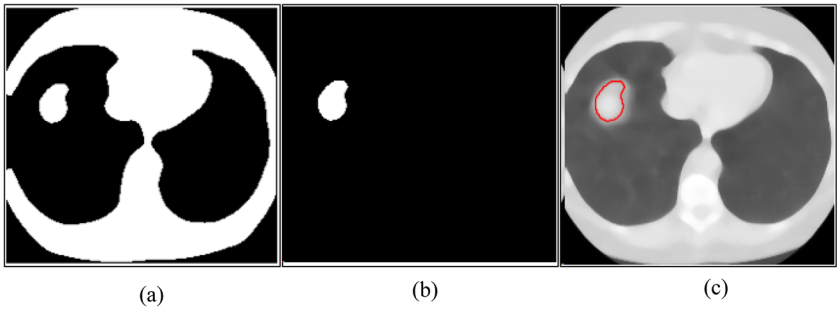

Fig. 3 Lung nodule segmentation **a** binarization **b** lung nodule **c** mapping

autoencoder and reinforcement [37] models for nodule prediction. The combination of handcrafted and deep features is also used for lung nodule prediction [38, 39].

Motivation

The proposed approach is motivated by lung cancer detection approach presented by Fernandes et al. [40]. In [40], the wavelet transform features were extracted from test data and local binary patterns (LBP) for quality assessment. They have used content supported medical image retrieval approach which is considered as best genetic optimization technique. The authors in [40] have also analyzed existing techniques which include K-nearest neighbor (KNN) [41], Naive-Bayes [42], Support Vector Machine (SVM) [43], bagging [44] and AdaBoost [45]. Their in-depth analysis is deliberated as a foundation in this field. Hence, in this article, the authors used decision trees (DT) [46], SVM, ensemble, KNN and softmax for classification.

Proposed approach

The lung CT images contain two regions of low and high intensity. For lung nodule, it is essential to isolate lung area from low intensity sections. As lung nodule has a complex structure, it is very much difficult to segment lung nodule more accurately. In this manuscript, median filter as an initial phase [47]. Otsu threshold and morphological erosion are used for lung nodule segmentation [48]. In the classification phase, deep features (VGG-19 model) along with handcrafted features are extracted. All these feature vectors are then fed to PCA for optimization and then serially fused [49]. The fused feature vector act as input for softmax layer to classify lung nodule. Fig. 1 depicts the proposed model overview.

Lesion enhancement and segmentation

Lesion enhancement is a vital step to boost the eminence of an input image φ(x, y), it helps to segment the particular area. 3D

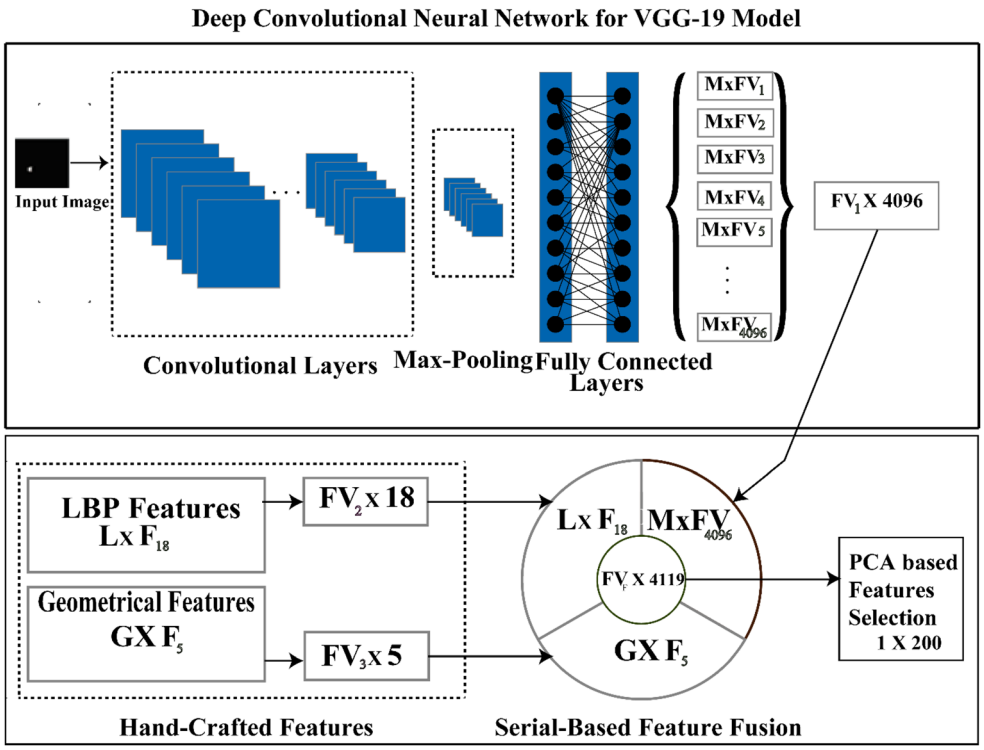

Fig. 4 Proposed model for feature extraction and fusion process for classification (FV denotes feature vector)

Table 1 Performance metrics

Performance measure	Equation
FNR	$FNR = \frac{FN}{FN+TP}$
FPR	$FPR = \frac{FP}{FP+TN}$
PPV	$PPV = \frac{TP}{TP+FP}$
SE	$SE = \frac{TP}{TP+FN}$
SP	$SP = \frac{TN}{TN+FP}$
ACC	$Accuracy = \frac{TP+TN}{TP+FN+FP+TN}$
AUC	$AUC = \int_{\infty}^{-\infty} TPR(T)FPR'(T)dT$

volume of lung slices is converted into grayscale$\varphi(x, y)_g$ for fast processing. The median filter $\varphi(x, y)_m$with 10×10 window size is used to smooth the input images as shown in depicted (Fig. 2).

The binarization is performed for the extraction of lung volume. The segmentation methods divide the image into separate regions $\varphi(x, y)_s$ having a homogeneous group of pixels which help to segment the lung nodule [50]. The lung nodule segmentation is carried out using thresholding. The threshold is optimized using Otsu method to maximize variance between the classes (σ_B).

$$\varphi(x, y)_{s\sigma_B(k^*)} = \max_{0 \le k \le l-1} (\sigma_B(k)) \quad (1)$$

In Eq. (1),$0 \le k \le l-1$ represents gray levels and k* denotes the optimal value of threshold. Moreover, morphological erosion with 10 arbitrary shape structuring elements is used to refine the segmented images as presented in Fig. 3.

$$\varphi(x, y)_{Erosion} \ominus B = \{z \in E | S_z \subseteq \varphi(x, y)_s\} \quad (2)$$

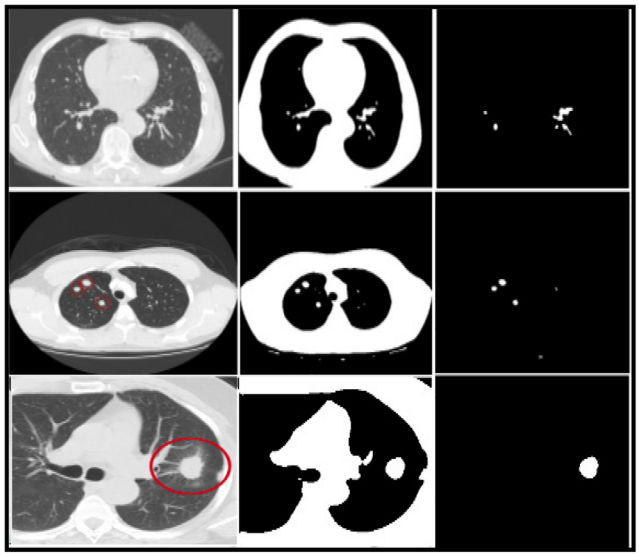

(a) (b) (c)

Fig. 5 Potential lung nodule on LIDC **a** input images **b** lung volumes corresponding to input image **c** lung nodule detection corresponding to input image

In Eq. (2), E represents an integer grid and B denotes the structuring element.

Feature extraction

In machine learning domain, extraction of features is an important task, which significantly effects the classification accuracy. Feature fusion method is used to create a new vector that contains more information as compared to a single feature vector. This manuscript highlights a hybrid/fused feature vector formed by the concatenation of geometrical, texture and deep learning features to provide better classification results. In the proposed method, 59 LBP, 05 geometrical and 4096 deep features are extracted, optimized and serially fused [51–53] as shown in Fig. 4.

Table 2 Classification results using Texture features

Classifier	Kernel	SE%	SP%	PPV%	FPR	FNR	ACC%	AUC
Softmax	Linear	0.93	1.00	1.00	0.00	0.06	0.95	0.92
Tree	Medium	0.93	0.50	0.82	0.50	0.06	0.81	0.83
	Coarse	0.75	1.00	1.00	0.00	0.24	0.80	0.79
SVM	Linear	0.77	0.83	0.93	0.16	0.22	0.79	0.84
	Quadratic	0.75	0.83	0.93	0.16	0.25	0.76	0.78
	Cubic	0.93	0.90	0.96	0.09	0.06	0.93	0.94
	Coarse Gaussian	0.93	0.76	0.90	0.23	0.06	0.88	0.87
KNN	Fine	0.96	1.00	1.00	0.00	0.03	0.97	0.96
	Cosine	0.93	0.83	0.93	0.16	0.06	0.90	0.92
	Cubic	0.84	0.44	0.67	0.55	0.16	0.67	0.69
Ensemble	Boosted	0.62	0.81	0.90	0.18	0.37	0.67	0.68
	Subspace	0.66	0.81	0.85	0.18	0.33	0.72	0.73

Table 3 Classification results using Deep features

Classifier	Kernel	SE%	SP%	PPV%	FPR	FNR	JSI	DSC	ACC%	AUC
Softmax	Linear	1.00	0.50	0.57	0.50	0.00	0.57	0.72	0.70	0.68
Tree	Medium	0.72	0.81	0.80	0.18	0.27	0.61	0.76	0.77	0.79
	Coarse	0.87	1.00	1.00	0.00	0.12	0.87	0.93	0.90	0.93
SVM	Linear	0.80	0.80	0.57	0.20	0.20	0.50	0.66	0.80	0.79
	Quadratic	0.77	1.00	1.00	0.00	0.22	0.77	0.87	0.80	0.82
	Cubic	0.85	0.66	0.85	0.33	0.14	0.75	0.85	0.80	0.82
	Coarse Gaussian	0.85	0.77	0.75	0.22	0.14	0.66	0.80	0.81	0.83
KNN	Fine	1.00	0.60	0.71	0.40	0.00	0.71	0.83	0.80	0.72
	Cosine	0.87	1.00	1.00	0.00	0.12	0.87	0.93	0.90	0.89
	Cubic	1.00	0.75	0.85	0.25	0.00	0.85	0.92	0.90	0.86
Ensemble	Boosted	0.66	0.75	0.80	0.25	0.33	0.57	0.72	0.70	0.67
	Subspace	0.87	0.75	0.87	0.25	0.12	0.77	0.87	0.83	0.79

Geometrical features

The geometrical [54] features are extracted from $\varphi(x, y)_{Erosion}$ including area, perimeter, eccentricity and diameter. Circularity is a useful feature because lung nodule appears in a circular shape. The extracted features are defined from Eq. (3) to Eq. (7).

$$\Phi(x,y)_{Erosion}(Area_R) = \sum_{i=x}^{x+width}\sum_{j=height}^{y+height} S_R(I,j) \quad (3)$$

$$\Phi(x,y)_{Erosion}(perimeter) = \sqrt{(x_2-x_1)^2 + (y_2-y_1)^2} \quad (4)$$

$$\varphi(x,y)_{Erosion}(Circularity\ ) = \frac{(4*Area*\pi)}{(perimeter^2)} \quad (5)$$

$$\varphi(x,y)_{Erosion}(Eccentricity) = \frac{1}{L1}\sqrt{(L1^2 + L2^2)} \quad (6)$$

$$\varphi(x,y)_{Erosion}(diameter) = \frac{\sqrt[3]{(diameter_L + diameter_S)*(diameter^2{}_L + diameter^2{}_S)}}{4} \quad (7)$$

Texture features

The texture features are more successfully used to detect lesion region because of encoding pixel wise texture pattern that provides more texture information. LBP texture feature with dimension 1×59 is extracted from $\varphi(x, y)_{Erosion}$ on which serial based feature subset selection method [53] is applied to select maximum 18 features by using PCA.

$$LBP\ \phi(x,y)_{\hat{P},R} = \sum_{i=0}^{\hat{P}-1} s(g_i - g_c)2^i \quad (8)$$

where

$$s(x) = \begin{cases} 1 & x \geq 0 \\ 0 & x < 0 \end{cases}$$

In Eq. (8), $\hat{P}$ denotes neighboring pixels, R depicts radius, $g_i$denotes intensities of neighborhood pixels and g_c represents central pixel values.

Table 4 Classification results using fused features

Classifier	Kernel	SE%	SP%	PPV%	FPR	FNR	JSI	DSC	ACC%	ROC
Softmax	Linear	0.93	1.00	1.00	0.00	0.06	0.93	0.96	0.95	0.94
Tree	Medium	0.96	0.98	0.97	0.00	0.03	0.94	0.97	0.97	0.98
	Coarse	0.89	0.99	0.97	0.00	0.10	0.87	0.93	0.95	0.93
SVM	Linear	0.99	1.00	1.00	0.00	0.009	0.99	0.99	0.99	0.97
	Quadratic	0.99	1.00	1.00	0.00	0.009	0.99	0.99	0.99	0.99
	Cubic	0.99	1.00	1.00	0.00	0.009	0.99	0.99	0.99	0.98
	Coarse Gaussian	0.98	1.00	1.00	0.00	0.018	0.98	0.99	0.98	0.99
KNN	Fine	0.98	0.98	0.96	0.01	0.011	0.95	0.97	0.98	0.98
	Cosine	1.00	0.88	0.93	0.11	0.000	0.93	0.96	0.95	0.96
	Cubic	0.99	1.00	1.00	0.00	0.009	0.99	0.99	0.99	0.99
Ensemble	Boosted	0.98	1.00	1.00	0.00	0.018	0.98	0.99	0.98	0.97
	Subspace	0.99	1.00	1.00	0.00	0.009	0.99	0.99	0.99	0.99

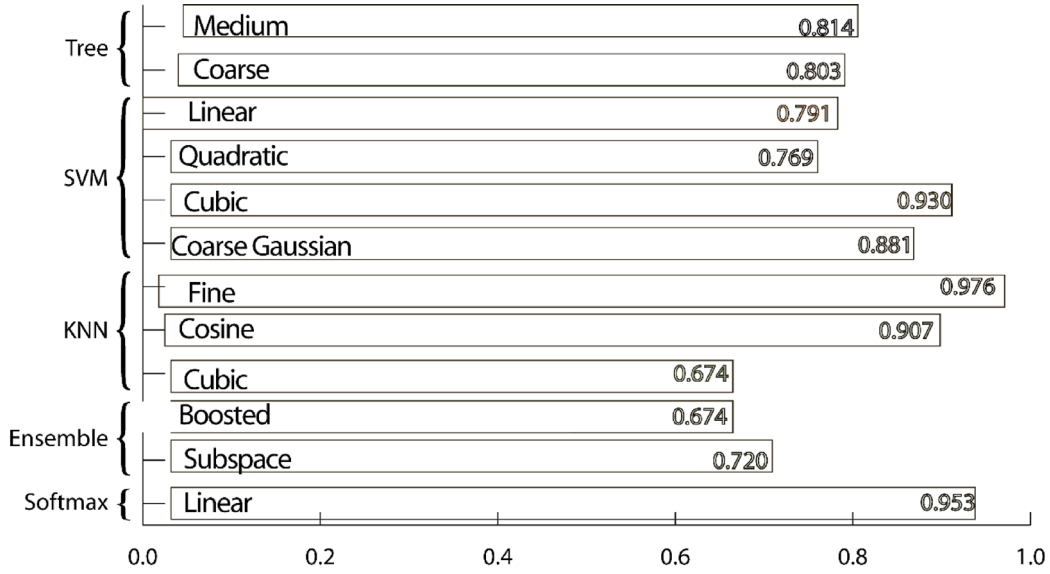

(a)

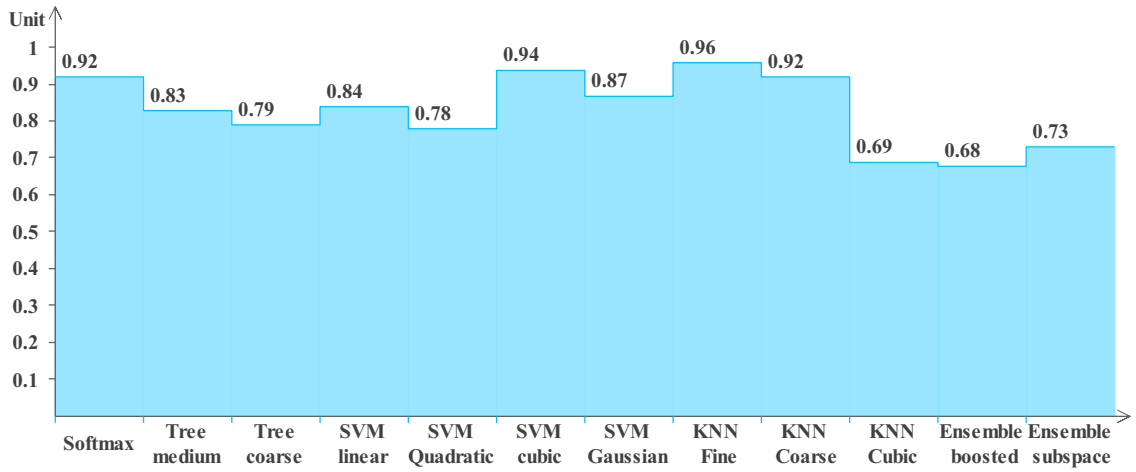

(b)

Fig. 6 Classification of lung nodule on texture features **a** classifiers accuracy **b** classifiers AUC

Deep learning features

VGG-19 is a CNN based model trained on Image Net dataset [55]. The segmented images are provided to this model to learn features automatically. To perform classification, softmax layer is used. The model consists of 19 layers including the input layer 240 × 240 × 1, 05 convolutional, 05 Rectified linear unit (ReLU), 05 max-pooling and 02 fully connected layers. The deep feature vector length is 1 × 4096.

Fused feature vector

The extracted features including deep features, LBP, geometric have total number of features are 4096, 59 and 5 respectively. Before fusing all these features, the PCA is applied on the respective feature sets with certain condition. This condition is to extract optimal features 177 out of 4096 from deep features, 18 out of 59 from LBP and all geometric features, which is then followed by fusion process. The fusion process have the final stage vector with the length 1 × 200.

Results and discussion

For classification, multiple classifiers are used including tree (medium, coarse) [46], SVM (linear, quadratic, cubic) [56–59], ensemble [60] (boosted, subspace), KNN [41] (fine, cosine, cubic) and softmax (linear) [61]. The

proposed work is implemented with MATLAB version 2018b on Intel 3.5 GHz with 32 GB RAM desktop computer. The benchmark dataset LIDC–IDRI is selected for the detection of lung nodule [62]. The dataset contains 1018 slices of 1010 cases of lung CT, where 777 scans of lung nodule and remaining non-nodule are utilized in this work because ground truth of these scans is available in XML sheet provided by the trained radiologists.

The performance evaluation is performed using accuracy (ACC), sensitivity (SE), specificity (SP), area under the curve (AUC), false negative rate (FNR), false positive rate (FPR) and positive predictive value (PPV). Table 1 mathematically depicts these evaluation measures.

TN, TP, FN, and FP represent true negative, true positive, false negative and false positive respectively. The proposed segmentation outcomes using LIDC–IDRI are presented in Fig. 5.

Experimentation

In this work, two different experiments are conducted to evaluate the results of this work. In the first experiment, handcrafted (geometrical, texture) and deep learning features (using VGG-19) are extracted from the segmented images. Then softmax and other state-of-the-art classifiers are considered to judge the nodule and non-nodule images.

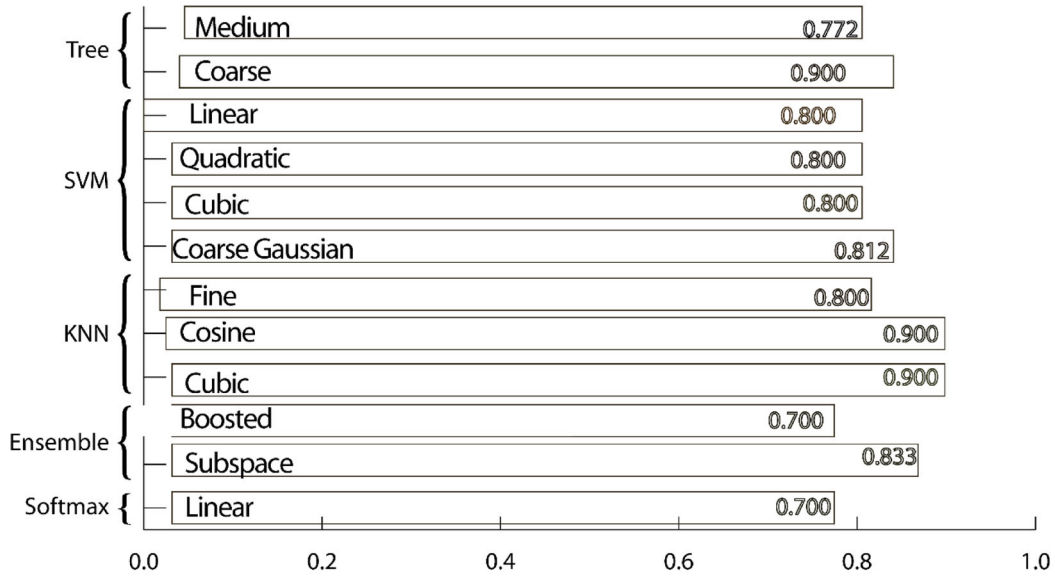

(a)

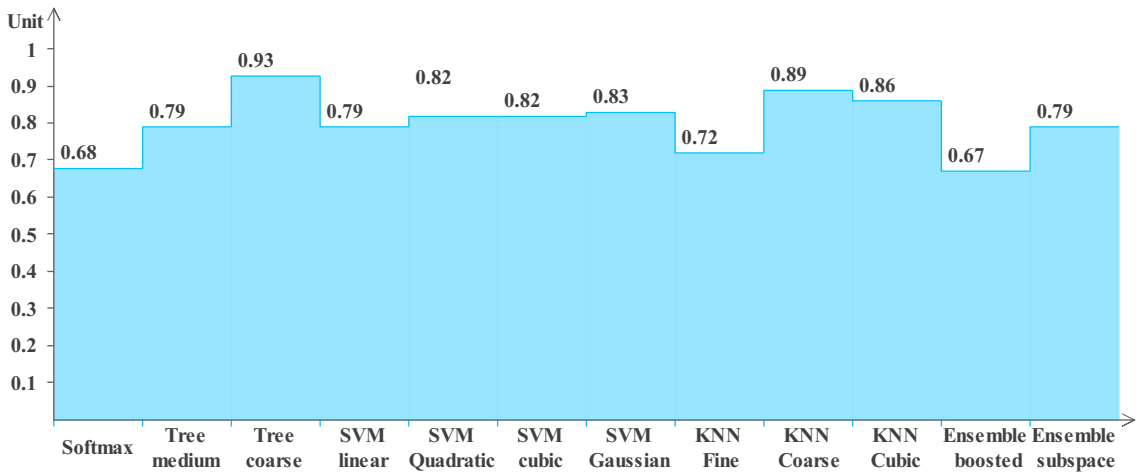

(b)

Fig. 7 Classification of lung nodule on deep features **a** classifiers accuracy **b** classifiers AUC

In the second experiment, deep learning models (Alex net [55], Google net [63], VGG-19 [64], residential energy services network (ResNet)-50 [65], *dense* convolutional network (Dense net-201) [66]) are applied to input lung images (without segmentation) for feature extraction. Afterwards, softmax is used to perform predictioln. For this, the transfer learning models are trained on 40 epochs. Although these models become stable most of the times after 30 epochs.

Experiment #1 (Classification with segmented images)

The results of proposed method using handcrafted texture and deep features are given in Tables 2 and 3 respectively. Whereas Table 4 presents the results of a fused feature vector that is combination of handcrafted and deep features.

On texture features, KNN classifier with fine kernel achieves 0.97 ACC and KNN with cubic and an ensemble with boosted kernel obtain 0.67 ACC. The maximum 0.96 AUC is achieved on a fine kernel of KNN and 0.94 AUC on a cubic kernel of SVM. The minimum 0.68 AUC is obtained on boosted kernel of ensemble classifier. Fig. 6 presents texture features results to evaluate accuracy and AUC.

On deep features, 0.90 ACC is achieved with KNN classifier (cosine and cubic) kernel whereas softmax with linear kernel and ensemble with boosted kernel obtain 0.70 ACC. The coarse kernel shows maximum AUC that is 0.93 on tree, 0.89 on KNN classifiers and minimum 0.67 on boosted kernel of ensemble

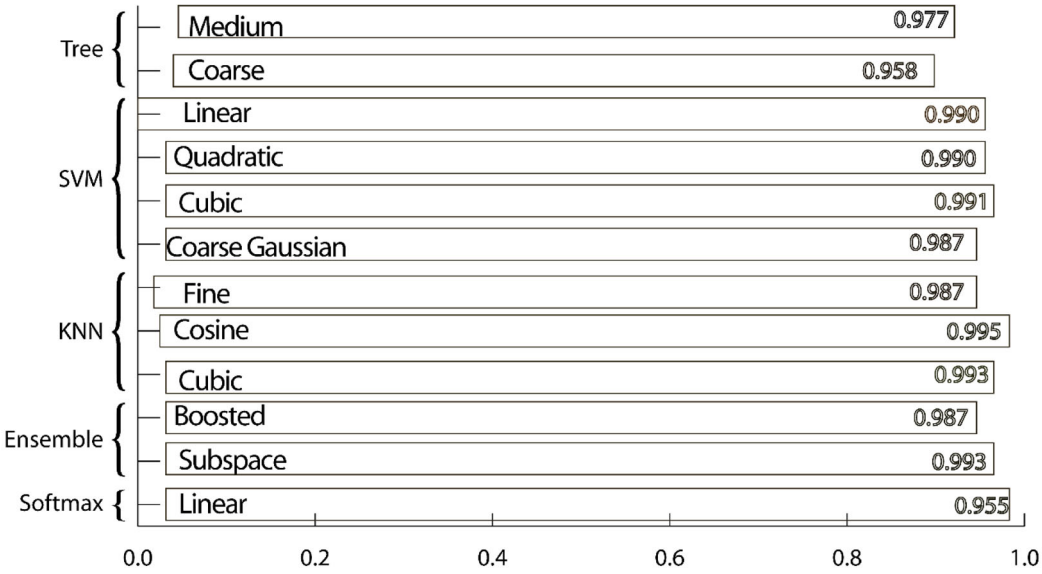

(a)

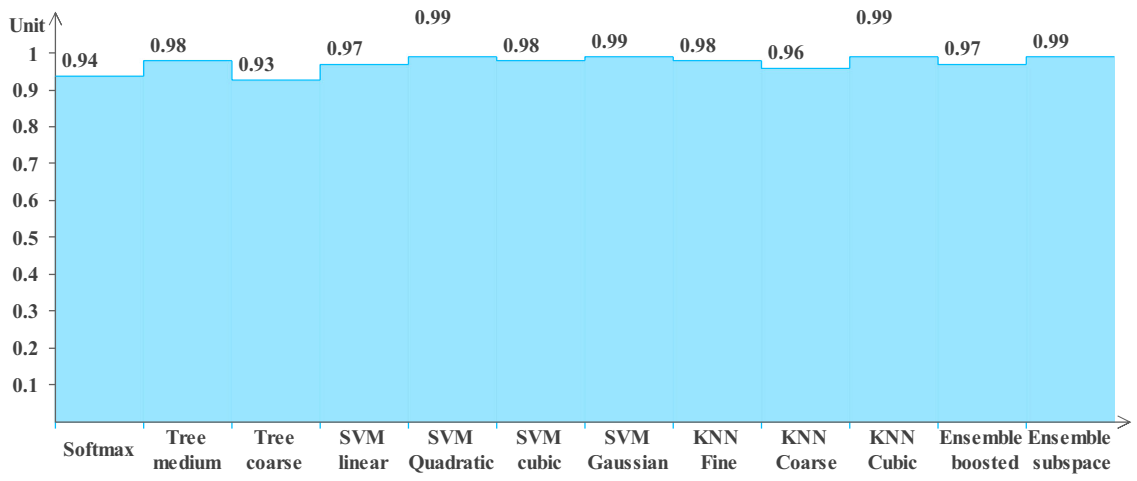

(b)

Fig. 8 Classification of lung nodule on the ensemble of texture and deep features **a** classifiers accuracy **b** classifiers AUC

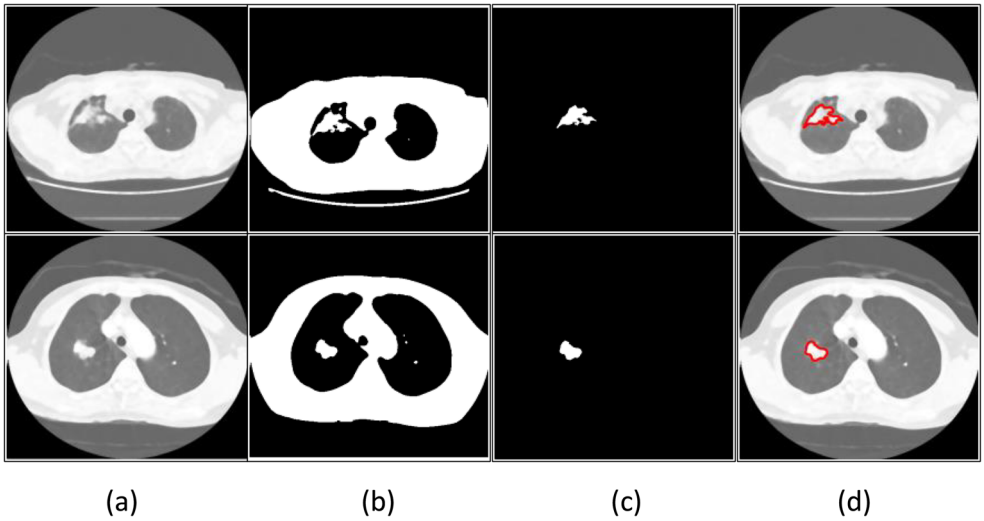

Fig. 9 Segmentation results using real patient images **a** input images **b** lung volume **c** lung nodule **d** mapping

Table 5 Proposed method comparison with existing approaches

Ref	Year	Dataset	ACC %	SE%	SP%
[35]	2017	LIDC–IDRI	0.89	0.91	0.88
[36]	2017	LIDC–IDRI	–	0.90	–
[68]	2018	LIDC–IDRI	0.99	0.98	0.98
[69]	2018	LIDC–IDRI	0.96	0.95	0.97
[70]	2019	LIDC–IDRI	0.84	–	–
Proposed results		LIDC–IDRI	0.99	0.99	1.00

classifier. The proposed approach results using deep features in terms of accuracy and AUC are shown in Fig. 7.

The evaluation depicts that fused features obtained greater classification accuracy when evaluated with individual feature vector in which KNN classifier with cubic kernel and ensemble with subspace kernel shows 0.99 ACC. The softmax obtains 1.00 SP and PPV using linear kernel. The maximum 0.99 AUC is attained using gaussian, quadratic kernels of SVM, cubic kernel of KNN and subspace kernel of ensemble classifiers. The presented method outcomes via a fusion of deep and texture features in terms of accuracy and AUC are shown in Fig. 8.

Fig. 9 presents the segmentation results evaluated on real patient images collected from Chang Bing Show Chwan Memorial Hospital (RD106070) and China Medical University Hospital (DMR-107-058) [67].

The proposed approach is assessed on separately extracted features that is texture, geometrical and deep features (using VGG 19) and fusion of these features. The experimental results demonstrate highest classification results on fused feature vector in comparison with individual features classification.

The presented method is also compared with existing methods (see Table 5) including ResNet [35] and 3D CNN [36], optimal threshold, seed growing, texture features, SVM [68], optimal threshold, hybrid features and a stacked autoencoder [69] for classifying the lung nodule. The comparison with current approaches presents the robustness of method presented in this manuscript.

Experiment #2 (Classification without segmentation)

In the second experiment, input images (without segmentation) act as an input to deep learning models so as to evaluate the results of classification. Alex net, Google net, Dense net 201, ResNet 50 and VGG-19 models are utilized for feature extraction and further fused with handcrafted features. The final fused vector is fed to softmax layer for classification (see Table 6).

Table 6 Classification results on transfer learning models (fusion of handcrafted and deep features)

	Deep learning models	SE%	SP%	PPV%	FPR	FNR	ACC%	AUC
Classification (without segmentation)	Alex net	0.87	0.66	0.77	0.33	0.12	0.78	0.86
	Google net	0.77	0.50	0.70	0.50	0.22	0.66	0.71
	Dense 201 net	0.75	0.85	0.75	0.14	0.25	0.81	0.80
	ResNet50	0.87	0.50	0.87	0.50	0.12	0.80	0.88
	VGG 19	0.76	0.74	0.81	0.25	0.23	0.75	0.70
With segmentation	VGG 19	0.76	0.74	0.81	0.25	0.23	0.75	0.70

It is evident from the above Table 6 that Densenet 201 net scores maximum 0.81 ACC while Google net shows minimum 0.66 ACC in classification without segmentation. Further, VGG-19 achieves an accuracy of 0.95 on the segmented images and 0.75 without segmentation. Overall, none of the models have attained maximum accuracy when compared to classification results based on segmentation.

Conclusion

This work used Otsu method using with the morphological operation to segment the lung nodule. In addition, texture, geometrical and deep features are extracted for optimization using PCA. The optimized feature vectors are serially fused for classifiers. This strategy works robustly to enhance the learning of classier when employed on unseen data. To conclude this work, the foremost objective is to reduce FP by preserving sensitivity. The results reflects that proposed technique on LIDC dataset obtains 0.99 SE with 0.01 FPR.

Future work

The proposed method classifies the lung nodule and non-nodule using Otsu segmentation and fusion of handcrafted and deep learning features. However, in future, semantic segmentation will be utilized for this purpose and results will be evaluated on real patient data that is helpful for the radiologists in the detection of lung nodule. This work can also be extended to other types of lung diseases by identifying disorders in tissue patterns for example unbalanced wall thickening of lung bullae.

Acknowledgments This work was supported by Research Project [Lung Cancer Diagnosis from CT Images]; Prince Sultan University; Saudi Arabia [SSP -18-5-03]". Additionally, this work was partially supported by Artificial Intelligence and Data Analytics (AIDA) Lab, Prince Sultan University, Riyadh, Saudi Arabia.

Funding information This work was supported by Research and Innovation Center through grant number SSP-18-5-03; Prince Sultan University, Riyadh, Saudi Arabia. This work was also partially supported by AI & Data Analytics Lab (AIDA), Prince Sultan University, Riyadh, Saudi Arabia.

Compliance with ethical standards

Conflict of interest All authors declare that they have no conflict of interest and all contribute equally in this work for results compilation and other technical support.

Ethical approval This work is based on publicly available datasets. This article does not contain any studies with human participants or animals performed by any of the authors.

Informed consent Not Applicable.

References

1. Gould, M. K., Fletcher, J., Iannettoni, M. D., Lynch, W. R., Midthun, D. E., Naidich, D. P., and Ost, D. E., Evaluation of patients with pulmonary nodules: when is it lung cancer?: ACCP evidence-based clinical practice guidelines. Chest 132(3):108S–130S, 2007.
2. Naqi, S., Sharif, M., Yasmin, M., and Fernandes, S. L., Lung nodule detection using polygon approximation and hybrid features from CT images. Current Medical Imaging Reviews 14(1):108–117, 2018.
3. Messay, T., Hardie, R. C., and Rogers, S. K., A new computationally efficient CAD system for pulmonary nodule detection in CT imagery. Med. Image Anal. 14(3):390–406, 2010.
4. Murphy, K., van Ginneken, B., Schilham, A. M., De Hoop, B., Gietema, H., and Prokop, M., A large-scale evaluation of automatic pulmonary nodule detection in chest CT using local image features and k-nearest-neighbour classification. Med. Image Anal. 13(5): 757–770, 2009.
5. Veronesi, G., Bellomi, M., Mulshine, J. L., Pelosi, G., Scanagatta, P., Paganelli, G., Maisonneuve, P., Preda, L., Leo, F., and Bertolotti, R., Lung cancer screening with low-dose computed tomography: a non-invasive diagnostic protocol for baseline lung nodules. Lung Cancer 61(3):340–349, 2008.
6. Kurihara, Y., Matsuoka, S., Yamashiro, T., Fujikawa, A., Matsushita, S., Yagihashi, K., and Nakajima, Y., MRI of pulmonary nodules. Am. J. Roentgenol. 202(3):W210–W216, 2014.
7. Amin, J., Sharif, M., Yasmin, M., and Fernandes, S. L., A distinctive approach in brain tumor detection and classification using MRI. Pattern Recogn. Lett., 2017.
8. Nida, N., Sharif, M., Khan, M. U. G., Yasmin, M., and Fernandes, S. L., A framework for automatic colorization of medical imaging. IIOAB J 7:202–209, 2016.
9. Amin, J., Sharif, M., Yasmin, M., and Fernandes, S. L., Big data analysis for brain tumor detection: Deep convolutional neural networks. Futur. Gener. Comput. Syst. 87:290–297, 2018.
10. Sobue, T., Moriyama, N., Kaneko, M., Kusumoto, M., Kobayashi, T., Tsuchiya, R., Kakinuma, R., Ohmatsu, H., Nagai, K., and Nishiyama, H., Screening for lung cancer with low-dose helical computed tomography: anti-lung cancer association project. J. Clin. Oncol. 20(4):911–920, 2002.
11. White, C., New techniques in thoracic imaging. Boca Raton: CRC Press, 2001.
12. Jiang, H., Ma, H., Qian, W., Gao, M., and Li, Y., An automatic detection system of lung nodule based on multigroup patch-based deep learning network. IEEE Journal of Biomedical and Health Informatics 22(4):1227–1237, 2018.
13. Ali I, Hart G, Gunabushanam G, Liang Y, Muhammad W, Nartowt B, Kane M, Ma X, Deng J (2018) lung nodule Detection via Deep reinforcement learning. Front. Oncol. 8:108
14. Thawani, R., McLane, M., Beig, N., Ghose, S., Prasanna, P., Velcheti, V., and Madabhushi, A., Radiomics and radiogenomics in lung cancer: a review for the clinician. Lung Cancer 115:34–41, 2018.
15. Li, C., Zhu, G., Wu, X., and Wang, Y., False-positive reduction on lung nodules detection in chest radiographs by ensemble of convolutional neural networks. IEEE Access 6:16060–16067, 2018.
16. M Naqi, S., and Sharif, M., Recent developments in computer aided diagnosis for lung nodule detection from CT images: a review. Current Medical Imaging Reviews 13(1):3–19, 2017.
17. Dehmeshki, J., Ye, X., Lin, X., Valdivieso, M., and Amin, H., Automated detection of lung nodules in CT images using shape-based genetic algorithm. Comput. Med. Imaging Graph. 31(6): 408–417, 2007.

18. Mattoccia, S., Tombari, F., and Di Stefano, L., Efficient template matching for multi-channel images. Pattern Recogn. Lett. 32(5): 694–700, 2011.
19. Ukil, S., and Reinhardt, J. M., Anatomy-guided lung lobe segmentation in X-ray CT images. IEEE Trans. Med. Imaging 28(2):202–214, 2009.
20. Han, H., Li, L., Han, F., Song, B., Moore, W., and Liang, Z., Fast and adaptive detection of pulmonary nodules in thoracic CT images using a hierarchical vector quantization scheme. IEEE journal of Biomedical and Health Informatics 19(2):648–659, 2015.
21. Gurcan, M. N., Sahiner, B., Petrick, N., Chan, H. P., Kazerooni, E. A., Cascade, P. N., and Hadjiiski, L., Lung nodule detection on thoracic computed tomography images: Preliminary evaluation of a computer-aided diagnosis system. Med. Phys. 29(11):2552–2558, 2002.
22. Lee, Y., Hara, T., Fujita, H., Itoh, S., and Ishigaki, T., Automated detection of pulmonary nodules in helical CT images based on an improved template-matching technique. IEEE Trans. Med. Imaging 20(7):595–604, 2001.
23. Dai, S., Lu, K., Dong, J., Zhang, Y., and Chen, Y., A novel approach of lung segmentation on chest CT images using graph cuts. Neurocomputing 168:799–807, 2015.
24. Firmino, M., Angelo, G., Morais, H., Dantas, M. R., and Valentim, R., Computer-aided detection (CADe) and diagnosis (CADx) system for lung cancer with likelihood of malignancy. Biomed. Eng. Online 15(1):2, 2016.
25. Ozekes, S., Osman, O., and Ucan, O. N., Nodule detection in a lung region that's segmented with using genetic cellular neural networks and 3D template matching with fuzzy rule based thresholding. Korean J. Radiol. 9(1):1–9, 2008.
26. Mukhopadhyay, S., A segmentation framework of pulmonary nodules in lung CT images. J. Digit. Imaging 29(1):86–103, 2016.
27. Gupta, A., Saar, T., Martens, O., and Moullec, Y. L., Automatic detection of multisize pulmonary nodules in CT images: Large-scale validation of the false-positive reduction step. Med. Phys. 45(3):1135–1149, 2018.
28. Keshani, M., Azimifar, Z., Tajeripour, F., and Boostani, R., Lung nodule segmentation and recognition using SVM classifier and active contour modeling: A complete intelligent system. Comput. Biol. Med. 43(4):287–300, 2013.
29. Ye, X., Lin, X., Dehmeshki, J., Slabaugh, G., and Beddoe, G., Shape-based computer-aided detection of lung nodules in thoracic CT images. IEEE Trans. Biomed. Eng. 56(7):1810–1820, 2009.
30. da Silva Sousa, J. R. F., Silva, A. C., de Paiva, A. C., and Nunes, R. A., Methodology for automatic detection of lung nodules in computerized tomography images. Comput. Methods Prog. Biomed. 98(1):1–14, 2010.
31. Teramoto, A., and Fujita, H., Fast lung nodule detection in chest CT images using cylindrical nodule-enhancement filter. Int. J. Comput. Assist. Radiol. Surg. 8(2):193–205, 2013.
32. Brown, M. S., Lo, P., Goldin, J. G., Barnoy, E., Kim, G. H. J., McNitt-Gray, M. F., and Aberle, D. R., Toward clinically usable CAD for lung cancer screening with computed tomography. Eur. Radiol. 24(11):2719–2728, 2014.
33. Riccardi, A., Petkov, T. S., Ferri, G., Masotti, M., and Campanini, R., Computer-aided detection of lung nodules via 3D fast radial transform, scale space representation, and Zernike MIP classification. Med. Phys. 38(4):1962–1971, 2011.
34. Gong, J., J-y, L., L-j, W., X-w, S., Zheng, B., and S-d, N., Automatic detection of pulmonary nodules in CT images by incorporating 3D tensor filtering with local image feature analysis. Physica Medica 46:124–133, 2018.
35. Nibali, A., He, Z., and Wollersheim, D., Pulmonary nodule classification with deep residual networks. Int. J. Comput. Assist. Radiol. Surg. 12(10):1799–1808, 2017.
36. Dou, Q., Chen, H., Yu, L., Qin, J., and Heng, P.-A., Multilevel contextual 3-d cnns for false positive reduction in pulmonary nodule detection. IEEE Trans. Biomed. Eng. 64(7):1558–1567, 2017.
37. Sun, W., Zheng, B., and Qian, W., Automatic feature learning using multichannel ROI based on deep structured algorithms for computerized lung cancer diagnosis. Comput. Biol. Med. 89:530–539, 2017.
38. Wang, C., Elazab, A., Wu, J., and Hu, Q., Lung nodule classification using deep feature fusion in chest radiography. Comput. Med. Imaging Graph. 57:10–18, 2017.
39. Xie, Y., Zhang, J., Xia, Y., Fulham, M., and Zhang, Y., Fusing texture, shape and deep model-learned information at decision level for automated classification of lung nodules on chest CT. Information Fusion 42:102–110, 2018.
40. Fernandes, S. L., Gurupur, V. P., Lin, H., and Martis, R. J., A Novel fusion approach for early lung cancer detection using computer aided diagnosis techniques. Journal of Medical Imaging and Health Informatics 7(8):1841–1850, 2017.
41. Peterson, L. E., K-nearest neighbor. Scholarpedia 4(2):1883, 2009.
42. Murphy, K. P., Naive bayes classifiers. Vol. 18. Vancouver: University of British Columbia, 2006, 60.
43. Burges, C. J., A tutorial on support vector machines for pattern recognition. Data Min. Knowl. Disc. 2(2):121–167, 1998.
44. Breiman, L., Bagging predictors. Mach. Learn. 24(2):123–140, 1996.
45. Sun, Y., Liu, Z., Todorovic, S., and Li, J., Adaptive boosting for SAR automatic target recognition. IEEE Trans. Aerosp. Electron. Syst. 43(1):112–125, 2007.
46. Swain, P. H., and Hauska, H., The decision tree classifier: Design and potential. IEEE Trans. Geosci. Electron. 15(3):142–147, 1977.
47. Lim, Jae S., Two-Dimensional Signal and Image Processing, Englewood Cliffs, NJ, Prentice Hall, 469–476, 1990.
48. Otsu, N., "A Threshold Selection Method from Gray-Level Histograms." IEEE Transactions on Systems, Man, and Cybernetics. 9(1):62–66, 1979.
49. Jolliffe, I. T. Principal Component Analysis. 2nd ed., Springer, 2002.
50. Despotović, I., Goossens, B., and Philips, W., MRI segmentation of the human brain: challenges, methods, and applications. Computational and Mathematical Methods in Medicine:1–23, 2015.
51. Ojala, T., M. Pietikainen, and T. Maenpaa. “Multiresolution Gray Scale and Rotation Invariant Texture Classification With Local Binary Patterns.” IEEE Transactions on Pattern Analysis and Machine Intelligence. 24(7):971–987, 2002.
52. https://www.mathworks.com/help/images/ref/regionprops.html#buoixjn-1. Accessed 2 Nov 2019.
53. Nasir, M., Attique Khan, M., Sharif, M., Lali, I. U., Saba, T., and Iqbal, T., An improved strategy for skin lesion detection and classification using uniform segmentation and feature selection based approach. Microsc. Res. Tech., 2018.
54. Lehmann, G., and Legland, D., Efficient N-dimensional surface estimation using Crofton formula and run-length encoding. Efficient N-Dimensional surface estimation using Crofton formula and run-length encoding, Kitware INC, 2012.
55. Krizhevsky, A., Sutskever, I., Hinton, G. E., Imagenet classification with deep convolutional neural networks. In: Advances in neural information processing systems, 2012. pp 1097–1105
56. Ansari, G. J., Shah, J. H., Yasmin, M., Sharif, M., and Fernandes, S. L., A novel machine learning approach for scene text extraction. Futur. Gener. Comput. Syst. 87:328–340, 2018.
57. Liaqat, A., Khan, M. A., Shah, J. H., Sharif, M., Yasmin, M., and Fernandes, S. L., Automated ulcer and bleeding classification from WCE images using multiple features fusion and selection. Journal of Mechanics in Medicine and Biology 18(04):1850038, 2018.

58. Sharif, M., Khan, M. A., Faisal, M., Yasmin, M., and Fernandes, S. L., A framework for offline signature verification system: Best features selection approach. Pattern Recogn. Lett., 2018.
59. Shah, J. H., Sharif, M., Yasmin, M., and Fernandes, S. L., Facial expressions classification and false label reduction using LDA and threefold SVM. Pattern Recogn. Lett., 2017.
60. Tumer, K., and Ghosh, J., Error correlation and error reduction in ensemble classifiers. Connect. Sci. 8(3–4):385–404, 1996.
61. Bishop, C. M. Pattern recognition and machine learning. springer, 2006.
62. Armato, III, S. G., McLennan, G., McNitt-Gray, M. F., Meyer, C. R., Yankelevitz, D., Aberle, D. R., Henschke, C. I., Hoffman, E. A., Kazerooni, E. A., and MacMahon, H., Lung image database consortium: developing a resource for the medical imaging research community. Radiology 232(3):739–748, 2004.
63. Szegedy, C., Liu, W., Jia, Y., Sermanet, P., Reed, S., Anguelov, D., Erhan, D., Vanhoucke, V., Rabinovich, A., Going deeper with convolutions. In: Proceedings of the IEEE conference on computer vision and pattern recognition, 2015. pp 1–9
64. Russakovsky, O., Deng, J., Su, H., Krause, J., Satheesh, S., Ma, S., Huang, Z., Karpathy, A., Khosla, A., and Bernstein, M., Imagenet large scale visual recognition challenge. Int. J. Comput. Vis. 115(3): 211–252, 2015.
65. He, K., Zhang, X., Ren, S., Sun, J., Deep residual learning for image recognition. In: Proceedings of the IEEE Conference on Computer Vision and Pattern Recognition, 2016. pp 770–778.
66. Huang G, Liu Z, Van Der Maaten L, Weinberger KQ Densely connected convolutional networks. In: Proceedings of the IEEE conference on computer vision and pattern recognition, 2017. pp 4700–4708
67. Chen, C.-H., Chang, C.-K., Tu, C.-Y., Liao, W.-C., Wu, B.-R., Chou, K.-T., Chiou, Y.-R., Yang, S.-N., Zhang, G., and Huang, T.-C., Radiomic features analysis in computed tomography images of lung nodule classification. PLoS One 13(2):e0192002, 2018. https://doi.org/10.1371/journal.pone.0192002.s001.
68. Naqi, S. M., Sharif, M., and Yasmin, M., Multistage segmentation model and SVM-ensemble for precise lung nodule detection. Int. J. Comput. Assist. Radiol. Surg.:1–13, 2018.
69. Naqi, S. M., Sharif, M., and Jaffar, A., Lung nodule detection and classification based on geometric fit in parametric form and deep learning. Neural Comput. & Applic.:1–19, 2018.
70. Bhatia, S., Sinha, Y., Goel, L., Lung Cancer Detection: A Deep Learning Approach. In: Soft Computing for Problem Solving. Springer, 2019, pp 699–705.